ADVANCED ELECTRONIC MATERIALS

Postfach 10 11 61
69451 Weinheim
Germany
Courier services:
Boschstraße 12
69469 Weinheim
Germany
Tel.: (+49) 6201 606 531
Fax: (+49) 6201 606 500
E-mail: advelectronicmat@wiley.com

WILEY-VCH

Dear Author,

Please correct your galley proofs carefully and return them no more than three days after the page proofs have been received.

If you have not used the PXE system before, please view the Tutorial before checking your proofs: http://wileypxe.aptaracorp.com/pxewileyvch/UserDocument/UserGuide/WileyPXE5_AuthorInstructions.pdf

Please note any queries that require your attention. These are indicated with red Qs in the pdf or highlighted as yellow queries in the "Edit" window.

Please pay particular close attention to the following, as no further corrections can be made once the article is published online:

- **Names** of all authors present and spelled correctly
- **Titles** of authors are correct (Prof. or Dr. only: please note, Prof. Dr. is not used in the journals)
- **Addresses of all authors** and **e-mail address of the corresponding author** are correct and up-to-date
- **Funding bodies** have been included and grant numbers are accurate
- The **Title** of the article is OK
- All **figures** are correctly included
- **Equations** are typeset correctly

Note that figure resolution in the PXE system is deliberately lower to reduce loading times. This will be optimized before the article is published online.

Please send any additional information, such as figures or other display items, to advelectronicmat@wiley.com, and please also indicate this clearly in the PXE "Edit" window by inserting a comment using the query tool.

Reprints may be ordered by filling out the accompanying form.
Return the reprint order form by e-mail with the corrected proofs, to Wiley- VCH: **advelectronicmat@wiley.com**

Please limit corrections to errors already in the text. Costs incurred for any further changes will be charged to the author, unless such changes have been agreed upon by the editor.

The editors reserve the right to publish your article without your corrections if the proofs do not arrive in time. Note that the author is liable for damages arising from incorrect statements, including misprints.

Editorial Office:
Wiley-VCH Verlag
Boschstraße 12, 69469 Weinheim
Germany

Tel.: (+49) 3047 031 331
Fax: (+49) 6201 606 500

Email: advelectronicmat@wiley.com

Reprint Order Form 2016

Short DOI: aelm. _____

Please send me and bill me for

no. of **Reprints** via ☐ airmail (+ 25 Euro)
☐ surface mail

Please send me and bill me for a

☐ **high-resolution PDF file** (330 Euro).

My Email address:

_____

Please note: It is not permitted to present the PDF file on the internet or on company homepages.

Information regarding VAT

Please note that from German sales tax point of view, the charge for **Reprints, Issues or Posters** is considered as **"supply of goods"** and therefore, in general, such delivery is a subject to German sales tax. However, this regulation has no impact on customers located outside of the European Union. Deliveries to customers outside the Community are automatically tax-exempt. Deliveries within the Community to institutional customers outside of Germany are exempted from the German tax (VAT) only if the customer provides the supplier with his/her VAT number. The VAT number (value added tax identification number) is a tax registration number used in the countries of the European Union to identify corporate entities doing business there. It starts with a country code (e.g. FR for France, GB for Great Britain) and follows by numbers.

VAT no.: _____

(Institutes / companies in EU countries only)

Purchase Order No.: _____

Delivery address / Invoice address:
Name of recipient, University, Institute, Street name and Street number, Postal Code, Country

_____

_____

_____

_____

_____

_____

_____

Date and Signature: _____

Credit Card Payment (optional) -You will receive an invoice.

VISA, MasterCard, AMERICAN EXPRESS

Please use the Credit Card Token Generator located at the website below to create a token for secure payment. The token will be used instead of your credit card number.

Credit Card Token Generator:
https://www.wiley-vch.de/editorial_production/index.php

Please transfer your token number to the space below.

Credit Card Token Number

Price list for reprints (The prices include mailing and handling charges. All Wiley-VCH prices are exclusive of VAT)

No. of pages	Price (in Euro) for orders of					
	50 copies	100 copies	150 copies	200 copies	300 copies	500 copies
1-4	345	395	425	445	548	752
5-8	490	573	608	636	784	1077
9-12	640	739	786	824	1016	1396
13-16	780	900	958	1004	1237	1701
17-20	930	1070	1138	1196	1489	2022
for every additional 4 pages	147	169	175	188	231	315

Wiley-VCH Verlag GmbH & Co. KGaA; Location of the Company: Weinheim, Germany;
Trade Register: Mannheim, HRB 432833, Chairman of the Board: Mark Allin
General Partner: John Wiley & Sons GmbH, Location: Weinheim, Germany
Trade Register Mannheim, HRB 432296, Managing Director: Sabine Steinbach

WILEY-VCH

Full Paper

xxxx

A. Lipatov, M. Alhabeb, M. R. Lukatskaya, A. Boson, Y. Gogotsi,* A. Sinitskii* .....x–xx

Effect of Synthesis on Quality, Electronic Properties and Environmental Stability of Individual Monolayer Ti_3C_2 MXene Flakes

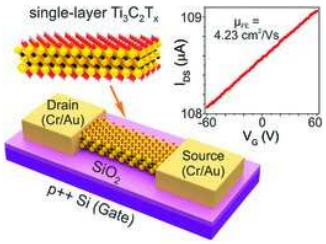

A synthetic method for high-quality monolayer flakes of $Ti_3C_2T_x$ is reported, the most studied MXene material, and the investigation of their electrical properties, environmental stability, and kinetics of oxidation in air. Individual monolayer $Ti_3C_2T_x$ flakes have electrical conductivity of 4600 ± 1100 S cm^{-1}, field-effect electron mobility of 2.6 ± 0.7 cm^{2}V^{-1}s^{-1}, and remain highly conductive even after exposure to air for more than 24 h.

aelm201600255(201600255)

www.advelectronicmat.de ADVANCED ELECTRONIC MATERIALS

Effect of Synthesis on Quality, Electronic Properties and Environmental Stability of Individual Monolayer Ti_3C_2 MXene Flakes

By *Alexey Lipatov, Mohamed Alhabeb, Maria R. Lukatskaya, Alex Boson, Yury Gogotsi,* and Alexander Sinitskii**

2D transition metal carbide $Ti_3C_2T_x$ (T stands for surface termination), the most widely studied MXene, has shown outstanding electrochemical properties and promise for a number of bulk applications. However, electronic properties of individual MXene flakes, which are important for understanding the potential of these materials, remain largely unexplored. Herein, a modified synthetic method is reported for producing high-quality monolayer $Ti_3C_2T_x$ flakes. Field-effect transistors (FETs) based on monolayer $Ti_3C_2T_x$ flakes are fabricated and their electronic properties are measured. Individual $Ti_3C_2T_x$ flakes exhibit a high conductivity of 4600 ± 1100 S cm^{-1} and field-effect electron mobility of 2.6 ± 0.7 cm^2 V^{-1} s^{-1}. The resistivity of multilayer $Ti_3C_2T_x$ films is only one order of magnitude higher than the resistivity of individual flakes, which indicates a surprisingly good electron transport through the surface terminations of different flakes, unlike in many other 2D materials. Finally, the fabricated FETs are used to investigate the environmental stability and kinetics of oxidation of $Ti_3C_2T_x$ flakes in humid air. The high-quality $Ti_3C_2T_x$ flakes are reasonably stable and remain highly conductive even after their exposure to air for more than 24 h. It is demonstrated that after the initial exponential decay the conductivity of $Ti_3C_2T_x$ flakes linearly decreases with time, which is consistent with their edge oxidation.

Q2 MXenes are a large family of 2D carbides and nitrides with a general formula $M_{n+1}X_nT_x$, where M stands for a transition metal, X is carbon and/or nitrogen, and T is a surface termination.[1] MXenes are produced from layered ternary metal carbides/nitrides, called MAX phases, by chemical extraction of interleaving layers of an "A" element (group IIIA and IVA elements, e.g., Al). Fluoride-containing acidic solutions, such as HF,[1,2] NH_4HF_2,[3] or LiF-HCl[4] are used for the A-element (typically, Al) extraction, which results in mixed oxygen- and fluorine-containing surface terminations. It was found that MXenes' surface chemistry,[5] conductivity,[3] capacitance,[4,6,7] and other properties are significantly affected by the synthesis method. For example, HF etching results in predominantly fluoride-containing functional groups, whereas LiF–HCl treatment yields material with mostly oxygen-containing surface groups.[8,9]

MXenes have demonstrated promise for a variety of applications and in particular for the energy storage in Li-ion,[1] Li-S,[10] Na-ion batteries,[11] and supercapacitors.[4,6] Yet the applications of this new family of the 2D materials in electronic devices, such as transistors and sensors, remains underdeveloped.[1,12–14] One of the reasons for this is lack of experimental data on electronic properties of single- and multi-layer MXenes. Electronic properties of the most widely studied MXene, $Ti_3C_2T_x$, were measured for bulk,[4,15] thin film,[3] or individual multilayer particles,[16] and only recently—individual flakes[17] (see Table S1 in the Supporting Information for a comparison). However, studies of other 2D materials, such as graphene,[18] phosphorene,[19] transition metal chalcogenides,[20] etc., have demonstrated the importance of characterizing electronic transport properties of individual monolayers and few-layer flakes. Furthermore, electronic properties of the 2D flakes strongly depend on the materials fabri-

A. Lipatov, A. Boson, A. Sinitskii, Department of Chemistry, University of Nebraska – Lincoln, Lincoln, NE 68588, USA
M. Alhabeb, M. R. Lukatskaya, Y. Gogotsi, Department of Materials Science and Engineering, Drexel University, Philadelphia, PA 19104, USA
M. Alhabeb, M. R. Lukatskaya, Y. Gogotsi, A. J. Drexel Nanomaterials Institute, Drexel University, Philadelphia, PA 19104, USA
A. Sinitskii, Nebraska Center for Materials and Nanoscience, University of Nebraska – Lincoln, Lincoln, NE 68588, USA
Correspondence to: Y. Gogotsi (E-mail: yg36@drexel.edu), A. Sinitskii (E-mail: sinitskii@unl.edu)
Q1
10.1002/aelm.201600255

ADVANCED ELECTRONIC MATERIALS

www.advelectronicmat.de

cation approaches and synthetic conditions. With little information that is currently available on the electrical properties of individual flakes of $Ti_3C_2T_x$, there is a limited understanding on how these properties depend on the approaches used for MXenes' synthesis. Further electrical characterization of individual $Ti_3C_2T_x$ flakes should establish the importance of the optimization of synthetic conditions for $Ti_3C_2T_x$, provide insights into its intrinsic properties, and reveal its potential for relevant applications.

For electronic property studies, controlled synthesis and delamination of MXenes into large monolayer flakes of high quality is required. High-yield delamination strategies depend on the synthesis method. MXenes produced by HF etching require an additional step of intercalation with organic molecules, such as DMSO[21] or amines,[22,23] whereas LiF–HCl etched MXene (also known as a "MXene clay") can be delaminated right away by sonication in water.[4]

The purpose of this study is manifold. First, we report on the transport property measurements of monolayer $Ti_3C_2T_x$ flakes. Second, we show that environmental stability of $Ti_3C_2T_x$ flakes strongly depends on their synthesis conditions. Particular attention has been paid to the optimization of LiF–HCl etching of Ti_3AlC_2 to produce high-quality MXene flakes with low concentration of defects. Finally, we demonstrate that electrical measurements can be used to study the kinetics of environmental degradation of $Ti_3C_2T_x$ flakes, which is an important issue for some of MXenes' potential applications.

Two types of $Ti_3C_2T_x$ flakes were produced for this study. Following the *original procedure* (Route 1) reported by Ghidiu et al.,[4] $Ti_3C_2T_x$ was synthesized by immersing Ti_3AlC_2 powder into an LiF–HCl solution maintaining the molar ratio of LiF to MAX equal to 5:1 (see Experimental Section for details). Previous studies have shown that this method yields primarily monolayer flakes.[4] In the *modified procedure* (Route 2), the molar ratio of LiF to MAX was increased to 7.5:1 to provide excess of Li^+ ions for intercalation and the HCl to LiF ratio was doubled to facilitate etching of aluminum. Other aspects of the procedure remained identical, except *no* sonication was needed to delaminate $Ti_3C_2T_x$ particles that were produced using Route 2 (see **Table 1**). Key differences between Routes 1 and 2 procedures are summarized in **Figure 1**A.

First, we evaluated the quality of $Ti_3C_2T_x$ flakes produced by different methods by electron microscopy techniques (Figure 1B–E). First, both solutions were drop-casted on silicon substrates characterized by scanning electron microscopy (SEM). The majority of the flakes produced by Route 1 are 200–500 nm in diameter (Figure 1B), and despite their small size some of the flakes are not completely exfoliated. In contrast, Route 2 MXene flakes are substantially larger, ranging from 4 to 15 μm in size (Figure 1D); they look uniform, have clean surfaces and the same brightness in the image, suggesting that they likely have the same thickness. Further characterization $Ti_3C_2T_x$ flakes produced by different methods was performed by transmission electron microscopy (TEM). Images of $Ti_3C_2T_x$ flakes prepared using Routes 1 and 2 are shown in Figure 1C,E, respectively. Low magnification images reveal that synthesis conditions significantly affect shape, size, and morphology of the flakes. $Ti_3C_2T_x$ flakes produced by Route 1 are smaller and have uneven edges decorated with tiny dark particles (Figure 1C), which we attribute to titanium dioxide, based on the results of prior studies.[24] In high resolution TEM images, $Ti_3C_2T_x$ flakes produced by Route 1 reveal numerous pin holes (Figure 1C). On the other hand, flakes produced using Route 2 are larger, have well-defined and clean edges and are visually hole-free (Figure 1E). Crystallographic shape of MXene flakes on TEM shows that MAX phase crystals can be delaminated without breaking the sheets. High-resolution TEM images that are presented in Figure 1C,E demonstrate hexagonal arrangement of atoms, showing that the crystal structure of both flakes is identical, which was further confirmed by selected area electron diffraction patterns. From this side-by-side comparison, it is clear that the modified synthesis procedure (Route 2) yields $Ti_3C_2T_x$ flakes of visibly higher quality and larger size compared to the flakes produced using Route 1. We attribute this improvement to the change in the composition of the etching solution, which facilitated both etching of aluminum and intercalation of lithium. As a result, multilayer $Ti_3C_2T_x$ flakes can be delaminated to monolayer flakes by a manual shake, with no need for sonication that shreds flakes into smaller pieces.

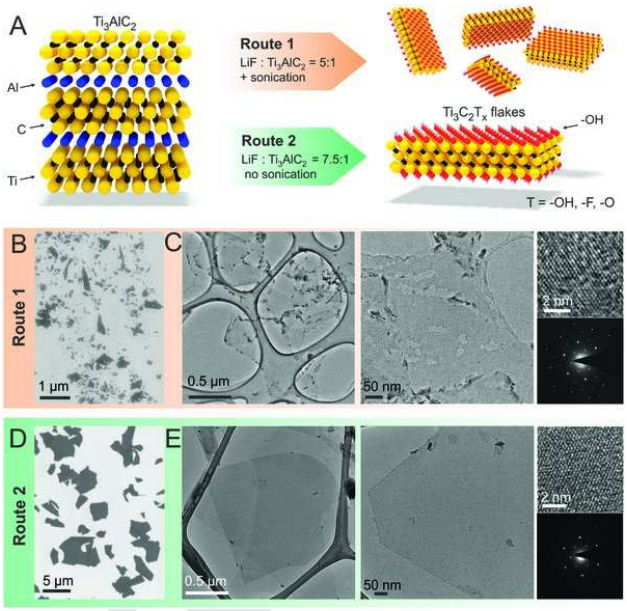

Figure 1. Synthesis and electron microscopy characterization of $Ti_3C_2T_x$ flakes produced by different routes. A) Summary of Routes 1 and 2 procedures and schematic structures of Ti_3AlC_2 and $Ti_3C_2T_x$. B) SEM and C) TEM images of $Ti_3C_2T_x$ flakes produced using Route 1. D) SEM and E) TEM images of $Ti_3C_2T_x$ flakes synthesized using Route 2. Small panels in (C) and (E) show HR TEM images and SAED patterns of monolayer 2D crystals of $Ti_3C_2T_x$.

The mechanical properties of $Ti_3C_2T_x$ MXenes produced by Routes 1 and 2 are quite different. Once MXene material is synthesized by either method, it is filtered on a PVDF membrane, forming a film (a "MXene paper"), which is then dried in a vacuum. Optical photographs of the filtrated films of $Ti_3C_2T_x$ MXenes produced by both Routes 1 and 2 are shown in **Figure 2**A. The MXene paper produced from the Route 1 $Ti_3C_2T_x$ can Q3

ADVANCED ELECTRONIC MATERIALS

Table 1. Summary of the experimental parameters for the original and modified etching/delamination procedures

	Weight (Ti_3AlC_2) [g]	Weight (LiF) [g]	Volume (6 M HCl) [mL]	Molar ratio Ti_3AlC_2:LiF:HCl	Etching time [h]	Centrifugation speed/time	Sonication
Original procedure ~~Route~~ 1	1	0.67	10	1.0:5.0:11.7	24	3500 rpm/1 h	Yes, 1 h
Modified procedure ~~Route~~ 2	1	1	20	1.0:7.5:23.4	24	3500 rpm/1 h	No

be easily ground to produce a fine black powder, see Figure 2A. However, more efforts are necessary to grind the filtrated $Ti_3C_2T_x$ film prepared by Route 2. Even shredding and more extensive grinding result in the material that consists of coarse shiny flakes, see Figure 2A. This is consistent with the results of SEM and TEM that demonstrate better exfoliation and larger flake size for the $Ti_3C_2T_x$ MXene material produced by Route 2, as large thin flakes are expected to stack better and form more mechanically stable structures.

Different stacking scenarios for the MXene flakes produced by two methods are manifested in the results of powder X-ray diffraction (XRD) measurements. Figure 2B shows that the XRD spectrum of the Route 2 $Ti_3C_2T_x$ flakes exhibits only a series of 00*l* reflections, indicating a layered structure of stacked flakes with an interplanar distance of 1.242 nm. In contrast, only 001 reflection is seen in the XRD pattern of the Route 1 $Ti_3C_2T_x$ flakes (Figure 2B), indicating that they form less ordered stacks compared to the flakes produced by Route 2. Also, this XRD pattern shows some peaks of the original MAX phase, which means that the transformation of MAX phase to MXene by Route 1 was not complete and some remaining incompletely exfoliated MAX particles are still present in the sample.

The thickness and shapes of the flakes produced by both methods was investigated by atomic force microscopy (AFM), see Figure 2C–G. The comparison of AFM images in Figure 2C and D presented at the same magnification shows that $Ti_3C_2T_x$ flakes synthesized by Route 2 are significantly larger compared to the material produced by Route 1. The AFM height profile measured along the blue dashed line in Figure 2D shows that all $Ti_3C_2T_x$ flakes have the same height of ≈ 2.7 nm and are identified as monolayers, as can be seen from Figure 2G that shows a folded $Ti_3C_2T_x$ flake produced by Route 2. The AFM height profile in the inset shows that the height of the folded region relative to the rest of the flake is ≈ 1.5 nm, which corresponds to a single layer of $Ti_3C_2T_x$ (according to DFT calculations and TEM studies, the thickness of an individual MXene flake is 0.98 nm[4,25]). However, the AFM height of the flake relative to the Si/SiO_2 substrate is 2.7 nm, as in case of Figure 2D,F. The increased height is likely due to the presence of surface adsorbates, such as water molecules, that are trapped under the $Ti_3C_2T_x$ flake; similar effects have been previously reported for other 2D materials as well.[26–29] In contrast, the AFM height profiles measured along the dashed lines in Figure 2C show that the flakes produced by Route 1 have different thicknesses (Figure 2E). ~~This observation further supports incomplete exfoliation of MAX phase *via* Route 1, which is consistent with the results obtained by other materials characterization methods.~~

The comparison of XPS spectra in the Ti 2p region for MXenes produced by Routes 1 and 2 ~~are~~ presented in Figure 2H. The fitting and analysis of the spectra was performed as described in previous works.[5,30,31] While the signals that are marked as C-Ti-T_x $2p_{3/2}$ and C-Ti-T_x $2p_{1/2}$[30] and correspond to Ti interactions with carbons and terminal atoms in $Ti_3C_2T_x$ look similar in both spectra, there is a visible increase in the signal intensities at ≈459 and ≈465 eV (these peaks are marked as TiO_2 $2p_{3/2}$ and TiO_2 $2p_{1/2}$, respectively),[31] which is another indication of oxidation of MXenes produced via Route 1.

To study electronic properties of $Ti_3C_2T_x$ flakes, we fabricated field-effect transistors (FETs) with individual MXene flakes as conductive channels. First, the diluted colloidal solution of $Ti_3C_2T_x$ flakes with concentration of about 0.01 mg mL^{-1} produced by Route 2 was drop-casted onto a Si/SiO_2 substrate. Similar to graphene and MoS_2, monolayer flakes of $Ti_3C_2T_x$ have a good optical contrast on a 300 nm SiO_2 on Si (see panel B in Figure S1 in the Supporting Information), so optical microscopy was used to establish flakes' position on the substrate. The largest flakes had the size of 5–8 μm and were uniform in color (no change in the number of layers), which made them suitable for device fabrication. After the flakes were selected, e-beam lithography was used for device patterning. Metal contacts composed of 3 nm of Cr and 20 nm of Au were deposited via e-beam evaporation. Special precautions were taken to avoid prolonged exposure of MXene flakes to air during device fabrication. Total time of the contact of the flakes with air was limited to ≈30 min from the moment of drop-casting to loading of the device into a vacuum chamber. **Figure 3**A shows the schematic illustration of the final $Ti_3C_2T_x$-based FET on Si/SiO_2 substrate where $Ti_3C_2T_x$ flake bridges Cr/Au source (S) and drain (D) electrodes, and back gate (G) electrode, a conductive highly p-doped Si, is separated from the MXene flake by 300 nm of SiO_2 dielectric. SEM images of a typical $Ti_3C_2T_x$ flake before and after device fabrication are shown in Figure 3B, additional SEM images of $Ti_3C_2T_x$ devices are provided in Figure S2 in the Supporting Information.

The electrical properties of Route 2 $Ti_3C_2T_x$ FETs were investigated for a total of four devices via the two-terminal method by measuring drain–source current (I_{DS}) while applying gate voltage (V_G) to the bottom electrode. Samples were kept at room temperature and drain–source voltage (V_{DS}) was 0.1 V to avoid Joule heating. In order to reduce the effect of surface adsorbates,[32] the measurements were performed in vacuum ($p \approx 2 \times 10^{-6}$ Torr) after two days of evacuation. I_{DS}–V_{DS} curves

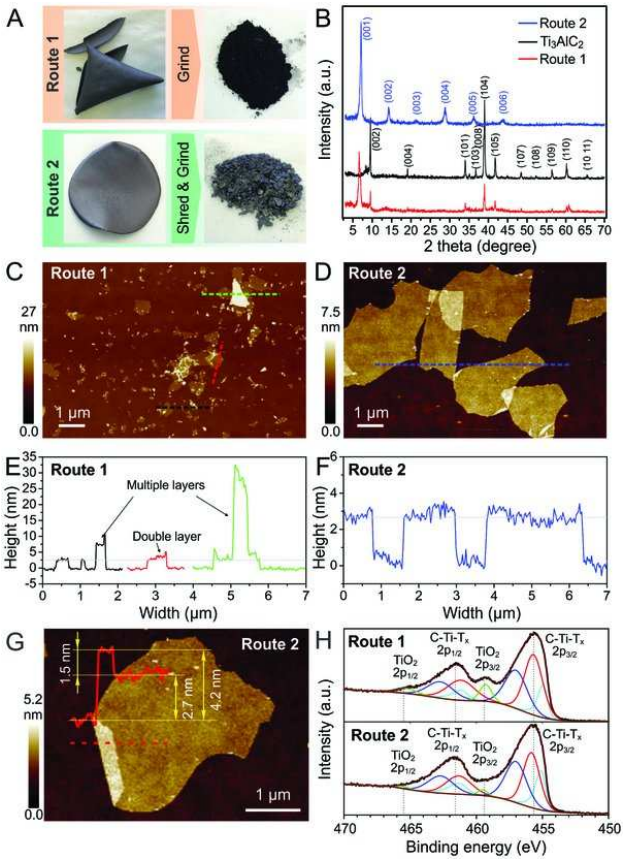

Figure 2. Comparison of $Ti_3C_2T_x$ materials produced by different routes. A) Optical photographs of MXene paper samples produced by different routes before and after grinding; see the text for details. B) XRD patterns collected for the powders of $Ti_3C_2T_x$ materials shown in panel A. XRD spectrum of the original Ti_3AlC_2 phase is shown as a reference. C,D) AFM images of the $Ti_3C_2T_x$ flakes deposited on Si/SiO_2: C) Route 1 and D) Route 2. E) AFM height profiles measured along the dashed lines in (C). The colors of the height profiles in (E) correspond to the colors of the dashed lines in (C). F) AFM height profile measured along the dashed line in (D). G) AFM image of a folded $Ti_3C_2T_x$ flake (Route 2) on Si/SiO_2. The inset shows the height profile measured along the red dashed line. H) Ti 2p XPS spectra of $Ti_3C_2T_x$ materials produced by Routes 1 and 2. Interactions of Ti with carbon and terminal atoms produce three signals (blue, red, and cyan fitting curves) that are collectively marked as C-Ti-T_x $2p_{3/2}$ and C-Ti-T_x $2p_{1/2}$. These signals correspond to different oxidation states of Ti. Titanium in TiO_2 produces distinctive signals at ≈459 and ≈465 eV (marked as TiO_2 $2p_{3/2}$ and TiO_2 $2p_{1/2}$).

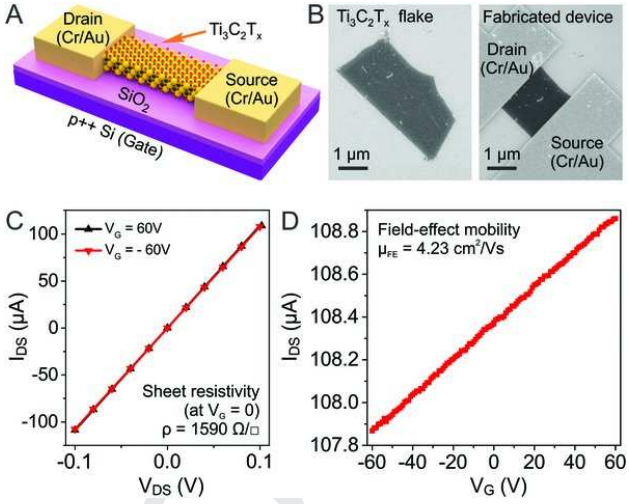

Figure 3. Device fabrication and electronic properties of $Ti_3C_2T_x$ flakes synthesized using Route 2. A) Schematic of a $Ti_3C_2T_x$-based FET; see the text for details. B) SEM image of a $Ti_3C_2T_x$ flake before and after device fabrication. C) $I_{DS}-V_{DS}$ curves for the device shown in (B) at different gate voltages. D) $I_{DS}-V_G$ dependence for the device shown in (B).

(Figure 3C) exhibit a linear dependence, which indicates ohmic behavior. Calculated sheet resistivity at $V_G = 0$ is $\rho = 1590\ \Omega\ \square^{-1}$. The results for other devices are summarized in Table S2 in the Supporting Information. The average resistivity for all measured devices is 2000±400 $\Omega\ \square^{-1}$, which is comparable to the sheet resistivity of graphene.[33] Since the thickness of the $Ti_3C_2T_x$ flake is 1 nm,[4,25] calculated single-flake resistivity is 2.04 ± 0.44 μΩ·m. We also performed resistivity measurements on the bulk $Ti_3C_2T_x$ clay using van der Paw method, see details in Supporting Information (Figure S3 and comments therein). $Ti_3C_2T_x$ film composed of exactly the same material as for monolayer property measurements revealed resistivity of 15.8 ± 1.3 μΩ·m. The difference between bulk and monolayer flake resistivities may be explained by the contribution of the contact resistance at the interfaces between individual MXene flakes, i.e., the resistance perpendicular to the basal plane. The difference between the resistivities of an individual monolayer $Ti_3C_2T_x$ flake and a film is within one order of magnitude, which is surprisingly small. In graphite, a stack of 2D sheets of graphene, the resistances perpendicular and parallel to the basal plane differs by three orders of magnitude.[34] In the recent study of $Ti_3C_2T_x$ particles,[16] the reported resistance anisotropy was also of about one order of magnitude. Moreover, the ratio strongly depended on the mechanical load (stretching or compressing) perpendicular to the basal plane, and comparable in- and out-of-plane resistances could be achieved when $Ti_3C_2T_x$ layers were pressed to each other.[16] These data as well as the results of our measurements demonstrate a good inter-flake conductance through the surface functional groups.

Application of external field via the gate electrode changes the Fermi level of MXene flakes, thus changing I_{DS}. As can be seen from Figure 3D, I_{DS} increases as V_G increases, indicating that electrons are major charge carriers. Leakage current is negligible (on the order of 10^{-11} A), so the electric field effect is intrinsic. $Ti_3C_2T_x$ field-effect electron mobility (μ_{FE}) was

Q5 estimated by fitting I_{DS}–V_G curve with Equation (1):[35]

$$\mu_{FE} = \frac{1}{C_G} \times \frac{d\left(1/\rho\right)}{d\,V_G}, \quad (1)$$

where C_G is a capacitance of the 300 nm SiO_2 dielectric layer. The resulting value of μ_{FE} for the device shown in Figure 3B is about 4.23 $cm^2\ V^{-1}\ s^{-1}$. The mobility is consistent across all measured devices with the average value of 2.6 ± 0.7 $cm^2\ V^{-1}\ s^{-1}$ (see Table S2 in the Supporting Information for the summary of the results of electrical measurements). We also attempted to improve the performance of devices by annealing them in Ar at 300 °C, but this did not have any significant effect on the conductivity and mobility values The distribution of the mobility values for MXene devices is rather narrow compared to a number of other solution-processed 2D materials, such as monolayer reduced graphene oxide (rGO) sheets[36] and nanoribbons,[37] suggesting the structural uniformity of $Ti_3C_2T_x$ flakes produced by Route 2. However, similarly to rGO monolayers, which due to defects and randomly distributed oxygen-containing functionalities have mobilities orders of magnitude lower than in pristine graphene,[36] non-periodic surface terminations (-OH, -F, -O)[8] in MXene flakes may negatively impact their mobilities. Also, SiO_2 surface and contaminations are known to contribute to mobility decrease in graphene due to electron–phonon[38] and Coulomb[35] scatterings. Encapsulation as well as dielectric screening can improve the mobility of $Ti_3C_2T_x$ devices, as shown for other 2D materials.[20, 39–42]

As we pointed out in the discussion of AFM results in Figure 2, monolayer $Ti_3C_2T_x$ flakes on Si/SiO_2 show step heights larger their expected thickness of ≈ 1 nm,[4, 25] which is likely due to the presence of surface adsorbates. Water molecules are known to cover SiO_2 thermally grown on Si in ambient conditions by hydrogen bonding to the surface Si–OH silanol groups.[43, 44] This hydrogen-bonded water cannot be completely desorbed by evacuation at room temperature, but can be removed by annealing at temperatures over 200 °C in dry environments.[45] In order to study the effect of adsorbed water on the electronic properties of $Ti_3C_2T_x$ devices, we annealed them at 300 °C in Ar for 30 min. This procedure resulted in the decrease of the AFM heights of the device channels from ≈ 2 to ≈1.5 nm (Figure S4, Supporting Information), which is comparable to the values measured for the relative thicknesses of folded regions of $Ti_3C_2T_x$ flakes (Figure 2G). The decrease in the AFM heights of $Ti_3C_2T_x$ channels after annealing is likely due to the thermal desorption of water. However, the annealing did not have a significant effect on the electronic properties of $Ti_3C_2T_x$ FETs, which remained qualitatively the same (see Figure S4 in the Supporting Information for details), so in the following experiments we discuss the results for devices prepared at room temperature.

Drop-casting of the $Ti_3C_2T_x$ colloidal solution produced following Route 1 onto Si/SiO_2 substrate mostly yielded non-uniform agglomerates of flakes which were not suitable for manufacturing devices with monolayer $Ti_3C_2T_x$ channels (see panel A in Figure S1 in the Supporting Information). Occasionally, small (< 5 μm) flakes could be spotted. Devices from $Ti_3C_2T_x$ flakes produced following Route 1 were fabricated using the same procedure as for Route 2 flakes, and representative SEM images of the devices are shown in Figure S5 in the Supporting Information. Electrical measurements of these FETs reveal the absence of I_{DS} dependence on V_{DS}, meaning that the flakes were not conductive. We explain the results by a higher oxidation degree of Route 1 flakes in comparison to Route 2 ones: pin-hole defects (Figure 1C) in flakes synthesized following Route 1 are likely to serve as nucleation sites for oxidation. These results, in combination with a lower quality of Route 1 flakes in TEM images (Figure 1C), demonstrate the importance of the synthesis procedure for manufacturing high-quality and environmentally stable flakes for electronic applications.

Monolayer MXene flakes cannot sustain prolonged exposure to oxygen in presence of water[24] or at high temperature.[46] Previous studies showed formation of titanium dioxide and carbon, with nucleation of titania crystals along the edges of MXene flakes.[46] For instance, when colloidal solution of delaminated MXene in water is exposed to air, $Ti_3C_2T_x$ flakes are completely oxidized within several days. This results in the solution color change from translucent black/brown to cloudy white, with a white precipitate of titania accumulating at the bottom of a vial. In this work, we studied kinetics of the environmental degradation of an individual $Ti_3C_2T_x$ flake in situ by measuring the change of FET's conductivity in air as a function of time. Device measurements have been previously used to study kinetics of other reactions involving 2D materials, such as diazonium functionalization of graphene.[47]

In these measurements we monitored the I_{DS} every 10 s, while exposing one of the previously discussed $Ti_3C_2T_x$ devices to air at room temperature and relative humidity ≈50%. **Figure 4**A shows the resulting time-dependence of I_{DS}. Black points at time (t) < 0 correspond to the readings in vacuum before the device was exposed to air. The readings are stable in vacuum but once the lid of a vacuum chamber is opened, the drain–source current started to decrease (see red data points in Figure 4A). The data were collected for 2.5 × 10^5 s (≈ 70 h) during which the I_{DS} decreased from 20.5 to 16.7 μA. The I_{DS} first decayed strongly in a non-linear manner within the initial ≈2 × 10^4 s, however, later, I_{DS} exhibited a linear decay over time. It should also be noted that linear dependence of I_{DS}–V_{DS} curves was preserved after the device was kept in air for 70 h, which indicates the degradation of $Ti_3C_2T_x$ flake rather than contacts between the flake and metal electrodes.

The observed decrease in the conductivity of a $Ti_3C_2T_x$ flake represents interplay of several different effects. First of all, we consider molecular adsorption on $Ti_3C_2T_x$ flakes (Figure 4B). It was previously shown that surface adsorbates may cause doping of 2D materials, such as graphene.[32, 48, 49] In case of air, particularly important adsorbates are oxygen and water molecules, both of which have been demonstrated to behave as electron acceptors when adsorbed on graphene resulting in p-doping.[48, 50] Since we demonstrate that electrons are the major charge carriers in $Ti_3C_2T_x$, its p-doping by surface adsorbates should result in a decrease in conductivity, which is consistent with our observations (Figure 4). Also, this conductivity change should be reversible if the molecules are desorbed from the surface of a $Ti_3C_2T_x$ flake in vacuum. In order to estimate the contribution of the molecular adsorbates to the overall

ADVANCED ELECTRONIC MATERIALS

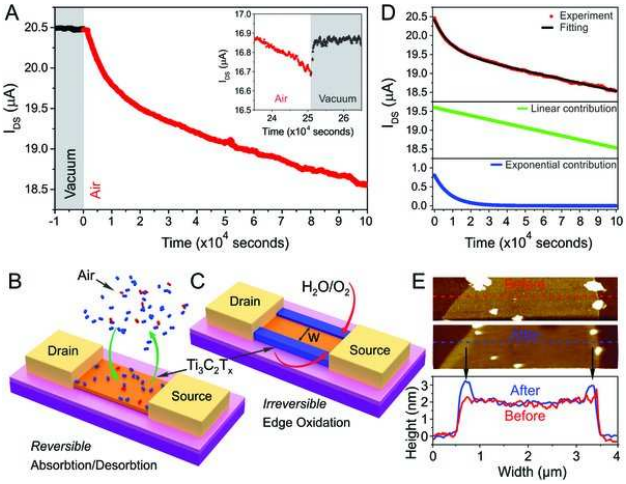

Figure 4. Environmental degradation of $Ti_3C_2T_x$ in air. A) Representative I_{DS}–time dependence for a $Ti_3C_2T_x$ FET exposed to air. The device was first kept under vacuum (black points) and then in air (red points). Fragment of the I_{DS}–time dependence for the same device, which shows partial restoration of the conductivity of the $Ti_3C_2T_x$ FET once it was evacuated. B,C) Schematic illustrations of phenomena that contribute to the decrease in the conductivity of $Ti_3C_2T_x$ devices in air: B) reversible molecular adsorption and C) irreversible edge oxidation; w represents the width of the conductive channel of the device that decreased due to the edge oxidation. D) Fit of the I_{DS}–time dependence shown in (A). Red data points show the experimental data and the black curve shows the fit. Both linear (green line) and exponential (blue line) contributions to the final fit (black line) are shown. E) AFM images of a fragment of the channel of a $Ti_3C_2T_x$ FET before and after the prolonged exposure to air, and height profiles measured along blue and red dashed lines in AFM images.

decrease in conductivity of the $Ti_3C_2T_x$ FET we measured the recovery of the I_{DS} in vacuum after the prolonged exposure of the device to air; see the inset in Figure 4A. After evacuation of the $Ti_3C_2T_x$ FET, the I_{DS} first increases but then saturates after ≈ 15 min, recovering only ≈0.8% (≈0.17 μA) of original I_{DS} value (compared to the overall 18.5% loss (3.79 μA) of I_{DS} during 70 h of the device exposure to air).

These results suggest that the major contribution to conductivity decrease in air is irreversible and thus likely related to the oxidation of $Ti_3C_2T_x$ flakes in air (Figure 4C). Oxidation of $Ti_3C_2T_x$ resulting in the formation of titanium dioxide has been discussed in previous studies[24] and is also illustrated by Figure 1. It is well known that oxidation of a 3D material often results in the formation of a passivating layer of a product that slows the reaction as it grows in thickness. The I_{DS}–time dependence that illustrates the kinetics of oxidation of a 2D MXene looks noticeably different (Figure 4A). In the first ≈2 × 10^4 s, the I_{DS}–time dependence shows an exponential decay and the oxidation rate indeed decreases with time, as expected. However, after the initial ≈2 × 10^4 s of exposure to air the oxidation rate does not decrease any further—it becomes constant and the I_{DS}–time dependence enters the linear regime (Figure 4A).

These observations can be rationalized as follows. In the beginning of the experiment the edges of $Ti_3C_2T_x$ flake are fully exposed to air and the oxidation proceeds rather quickly. Titanium dioxide, formed at the edges of the flake, slows the reaction at first. However, further kinetics is different from the oxidation kinetic of a 3D material, where the oxidation product passivates the entire surface of a material and the reaction rate decreases as oxide layer become thicker. In case of the 2D edge oxidation of $Ti_3C_2T_x$, the titanium oxide that forms at the sides of a flake does not fully passivate the material from the environment (Figure 4C). Furthermore, once the edges of the flakes are oxidized and the reaction is slowed down to a certain extent, then the oxidation should proceed with a nearly constant rate, because the oxidizing species diffuse not through the oxide layer, like in 3D case, but directly at the $Ti_3C_2T_x/TiO_2$ interface (Figure 4C). We have recorded I_{DS}–time dependencies for several $Ti_3C_2T_x$ FETs exposed to air, and in all cases after the initial exponential decay we observed a linear decrease in conductivity with time, which is consistent with the described model. We believe that similar kinetics could be observed for reactions involving other 2D materials as well, particularly when the reactions primarily happen at the edges rather than on the basal plane.

To further illustrate the transition from exponential decay to linear regime, we fitted the experimental data using the following equation:

$$I_{DS}(t) = A - B \cdot t + C \cdot \exp(-\gamma \cdot t), \quad (2)$$

where A, B, C, and γ are the fitting parameters. The fit worked very well in the entire time range as shown in the top panel in Figure 4D. The values extracted by fitting the experimental data with Equation (2) are $A = 19.599(2)$, $B = 1.068(3) \times 10^{-5}$, $C = 0.810(3)$, and $\gamma = 1.16(1) \times 10^{-4}$. The middle and bottom panels in Figure 4D demonstrate individual contributions of linear and exponential parts of Equation (2). They further demonstrate that the exponential term initially dominates, but then the contribution of the linear term becomes more important.

Edges of $Ti_3C_2T_x$ flakes and other structural defects (Ti vacancies and pin holes) are the most vulnerable sites for oxidation. For the $Ti_3C_2T_x$ flakes with high structural quality (prepared by Route 2), it is reasonable to assume that the edge oxidation will proceed faster than the oxidation at the basal plane and thus will make the largest contribution to the overall conductivity decrease. This scenario is illustrated by Figure 4C that shows that the edge oxidation decreases the width of the $Ti_3C_2T_x$ FET channel (w), which results in the conductivity decrease. To verify this assumption, we compared AFM images of as-prepared $Ti_3C_2T_x$ FETs with AFM images of the same device after prolonged exposure to air. Figure 4E shows that the $Ti_3C_2T_x$ channel of as-prepared device has a uniform thickness of ≈ 2 nm. After exposure to air the flake becomes visibly thicker at the edges, but the thickness does not change at the basal plane. This observation is consistent with the assumption that the environmental degradation primarily happens at

ADVANCED ELECTRONIC MATERIALS

the exposed edges of the $Ti_3C_2T_x$ flake, while the basal plane is reasonably inert to oxidation. The height profiles measured along the same portion of the $Ti_3C_2T_x$ channel before and after exposure to air for 70 h show that the flake thickness increases at the edges by ≈ 1 nm (see arrows in Figure 4E). The AFM data confirm the conclusion made from the results of electrical measurements that environmental degradation of high-quality $Ti_3C_2T_x$ flakes is reasonably slow. Since the oxidized edges are less conductive than the interiors of $Ti_3C_2T_x$ flakes, they could be visualized by scanning electron microscopy. SEM images of $Ti_3C_2T_x$ flakes that were deposited on Si/SiO_2 substrates and exposed to air for several days show that the edges of flakes are visibly brighter than their interiors (Figure S6, Supporting Information)—such contrast was not observed for the $Ti_3C_2T_x$ flakes that were imaged shortly after their deposition on Si/SiO_2 substrates, see Figure 1B,D.

The sensitivity of the conductivity of $Ti_3C_2T_x$ to molecular adsorbates and some reversibility of the process suggest the potential of this material and other MXenes for sensor applications. Previously, different kinds of sensors were demonstrated for many other 2D materials, such as graphene, graphene oxide, and transition metal chalcogenides; which benefit from high surface-to-volume ratios and tunable electronic properties.[51,52] Very rich surface chemistry of MXenes with about 20 compositions of various transition metals and their combinations available to date[53,54] makes MXene FETs promising for sensing applications as well. Of course, the environmental degradation could be a serious issue for such sensors. However, considering that the oxidation of high-quality $Ti_3C_2T_x$ flakes primarily happens at the edges, this issue could be mitigated by passivating edges with inert oxide materials using, for example, a technique like atomic layer deposition, or encapsulating them with impermeable 2D materials, such as hexagonal boron nitride (h-BN).

In summary, we demonstrate an improved method of selective etching of Ti_3AlC_2, a MAX phase, which yields high-quality monolayer $Ti_3C_2T_x$ MXene flakes with well-defined and clean edges and visually defect-free surfaces. We fabricated FETs based on monolayer $Ti_3C_2T_x$ flakes, which exhibited a field-effect electron mobility of 2.6 ± 0.7 cm^2 V^{-1} s^{-1} and a low resistivity of 2.31 ± 0.57 μΩ·m (4600 ± 1100 S cm^{-1}). The single flake resistivity is only one order of magnitude higher than the resistivity of bulk $Ti_3C_2T_x$ and thin films made from $Ti_3C_2T_x$ flakes, suggesting that $Ti_3C_2T_x$ flakes form low-resistance electric contacts with each other, which is a practically important result for bulk applications of this material. Finally, we used fabricated FETs to investigate the environmental stability of $Ti_3C_2T_x$ flakes in humid air. The high-quality $Ti_3C_2T_x$ flakes are reasonably stable and remain highly conductive even after their exposure to air for 70 h. After the initial exponential decay the drain–source current linearly decreases with time. We explain these observations by the edge oxidation of $Ti_3C_2T_x$ flakes and support this explanation by AFM measurements. We believe that similar kinetics could be observed for reactions involving other 2D materials as well, in cases when the reactions primarily happen at the edges rather than on the basal plane. Many of such kinetics studies of other conductive 2D materials may potentially be carried out using the electrical measurement scheme that was disclosed in this paper.

Experimental Section

Synthesis of $Ti_3C_2T_x$ Following the Original[4] and Modified Procedure: MAX phase precursor, Ti_3AlC_2, was produced as described elsewhere.[4] Following the procedure in Ghidiu et al.,[4] 0.67 g of LiF was dissolved in 10 mL of 6 M HCl and the solution was allowed to mix thoroughly at room temperature for a few minutes. After that, 1 g of Ti_3AlC_2 was slowly added over the course of 5 min to avoid initial overheating due to exothermic nature of the reaction. Then, the temperature was brought to 35 °C and the reaction allowed to proceed under continuous stirring (550 rpm) for 24 h. The resulting MXene powder was repeatedly washed with DI water until almost neutral pH (≥ 6). The product was then collected using vacuum-assisted filtration through a PVDF membrane (0.45 μm pore size, Millipore) and dried in a vacuum desiccator at room temperature for 24 h. To delaminate 0.2 g of $Ti_3C_2T_x$, the freshly produced powder was bath sonicated in 50 mL of DI water for 1 h under continuous argon (Ar) bubbling to minimize oxidation. Then, the $Ti_3C_2T_x$ solution was centrifuged at 3500 rpm for 1 h and the supernatant, a colloidal solution of MXene, was collected. Previous studies have shown that this solution contains primarily monolayer flakes.[4] In the *modified procedure*, 1 g of MAX was added to the mixture of 1 g of LiF in 20 mL of 6 M HCl. Other aspects of the procedure remained identical except delamination of the resulting $Ti_3C_2T_x$ powder did not require sonication (Table 1).

Supporting Information

Supporting Information is available from the Wiley Online Library or from the author.

Acknowledgements

All the authors contributed equally to this work and have given approval to the final version of the manuscript. This work was supported by the National Science Foundation (NSF) through ECCS-1509874 with a partial support from the Nebraska Materials Research Science and Engineering Center (MRSEC) (grant no. DMR-1420645). Materials synthesis at Drexel University was supported by the Fluid Interface Reactions, Structures and Transport (FIRST) Center, the Energy Frontier Research Center funded by the U.S. Department of Energy, Office of Science, Office of Basic Energy Sciences. The authors declare no competing financial interests.

Q6

Received: July 2, 2016
Revised: July 26, 2016
Published Online: MM DD, YYYY

[1] M. Naguib, V. N. Mochalin, M. W. Barsoum, Y. Gogotsi, *Adv. Mater.* **2014**, *26*, 992,
[2] M. Naguib, M. Kurtoglu, V. Presser, J. Lu, J. J. Niu, M. Heon, L. Hultman, Y. Gogotsi, M. W. Barsoum, *Adv. Mater.* **2011**, *23*, 4248.

ADVANCED ELECTRONIC MATERIALS

[3] J. Halim, M. R. Lukatskaya, K. M. Cook, J. Lu, C. R. Smith, L. A. Naslund, S. J. May, L. Hultman, Y. Gogotsi, P. Eklund, M. W. Barsoum, *Chem. Mater.* **2014**, *26*, 2374.
[4] M. Ghidiu, M. R. Lukatskaya, M. Q. Zhao, Y. Gogotsi, M. W. Barsoum, *Nature* **2014**, *516*, 78.
[5] J. Halim, K. M. Cook, M. Naguib, P. Eklund, Y. Gogotsi, J. Rosen, M. W. Barsoum, *Appl. Surf. Sci.* **2015**, *362*, 406.
[6] M. R. Lukatskaya, O. Mashtalir, C. E. Ren, Y. Dall'Agnese, P. Rozier, P. L. Taberna, M. Naguib, P. Simon, M. W. Barsoum, Y. Gogotsi, *Science* **2013**, *341*, 1502.
[7] Y. Dall'Agnese, M. R. Lukatskaya, K. M. Cook, P. L. Taberna, Y. Gogotsi, P. Simon, *Electrochem. Commun.* **2014**, *48*, 118.
[8] H.-W. Wang, M. Naguib, K. Page, D. J. Wesolowski, Y. Gogotsi, *Chem. Mater.* **2016**, *28*, 349.
[9] M. A. Hope, A. C. Forse, K. J. Griffith, M. R. Lukatskaya, M. Ghidiu, Y. Gogotsi, C. P. Grey, *Phys. Chem. Chem. Phys.* **2016**, DOI: 10.1039/c6cp00330c.
Q7
[10] X. Liang, A. Garsuch, L. F. Nazar, *Angew. Chem. Int. Ed.* **2015**, *54*, 3907.
[11] X. Wang, S. Kajiyama, H. Iinuma, E. Hosono, S. Oro, I. Moriguchi, M. Okubo, A. Yamada, *Nat. Commun.* **2015**, *6*, 6544.
[12] J. Chen, K. Chen, D. Tong, Y. Huang, J. Zhang, J. Xue, Q. Huang, T. Chen, *Chem. Commun.* **2015**, *51*, 314.
[13] S. Lai, J. Jeon, S. K. Jang, J. Xu, Y. J. Choi, J.-H. Park, E. Hwang, S. Lee, *Nanoscale* **2015**, *7*, 19390.
[14] C. Xu, L. Wang, Z. Liu, L. Chen, J. Guo, N. Kang, X.-L. Ma, H.-M. Cheng, W. Ren, *Nat. Mater.* **2015**, *14*, 1135.
[15] M. Naguib, O. Mashtalir, J. Carle, V. Presser, J. Lu, L. Hultman, Y. Gogotsi, M. W. Barsoum, *ACS Nano* **2012**, *6*, 1322.
[16] T. Hu, H. Zhang, J. Wang, Z. Li, M. Hu, J. Tan, P. Hou, F. Li, X. Wang, *Sci. Rep.* **2015**, *5*, 16329.
[17] A. Miranda, J. Halim, M. W. Barsoum, A. Lorke, *Appl. Phys. Lett.* **2016**, *108*, 033102.
[18] K. S. Novoselov, A. K. Geim, S. V. Morozov, D. Jiang, Y. Zhang, S. V. Dubonos, I. V. Grigorieva, A. A. Firsov, *Science* **2004**, *306*, 666.
[19] H. Liu, A. T. Neal, Z. Zhu, Z. Luo, X. Xu, D. Tománek, P. D. Ye, *ACS Nano* **2014**, *8*, 4033.
[20] B. Radisavljevic, A. Radenovic, J. Brivio, V. Giacometti, A. Kis, *Nat. Nanotechnol.* **2011**, *6*, 147.
[21] O. Mashtalir, M. Naguib, V. N. Mochalin, Y. Dall'Agnese, M. Heon, M. W. Barsoum, Y. Gogotsi, *Nat. Commun.* **2013**, *4*, 1716.
[22] O. Mashtalir, M. R. Lukatskaya, M. Q. Zhao, M. W. Barsoum, Y. Gogotsi, *Adv. Mater.* **2015**, *27*, 3501.
[23] M. Naguib, R. R. Unocic, B. L. Armstrong, J. Nanda, *Dalton Trans.* **2015**, *44*, 9353.
[24] O. Mashtalir, K. M. Cook, V. N. Mochalin, M. Crowe, M. W. Barsoum, Y. Gogotsi, *J. Mater. Chem. A* **2014**, *2*, 14334.
[25] X. Wang, X. Shen, Y. Gao, Z. Wang, R. Yu, L. Chen, *J. Am. Chem. Soc.* **2015**, *137*, 2715.
[26] K. S. Novoselov, D. Jiang, F. Schedin, T. J. Booth, V. V. Khotkevich, S. V. Morozov, A. K. Geim, *Proc. Natl. Acad. Sci. USA* **2005**, *102*, 10451.
[27] K. Xu, P. Cao, J. R. Heath, *Science* **2010**, *329*, 1188.
[28] O. Ochedowski, B. K. Bussmann, M. Schleberger, *Sci. Rep.* **2014**, *4*, 6003.
[29] H. Coy Diaz, R. Addou, M. Batzill, *Nanoscale* **2014**, *6*, 1071.
[30] C. E. Ren, M.-Q. Zhao, T. Makaryan, J. Halim, M. Boota, S. Kota, B. Anasori, M. W. Barsoum, Y. Gogotsi, *ChemElectroChem* **2016**, *3*, 689.
[31] Z. Song, J. Hrbek, R. Osgood, *Nano Lett.* **2005**, *5*, 1327.
[32] A. Sinitskii, A. Dimiev, D. V. Kosynkin, J. M. Tour, *ACS Nano* **2010**, *4*, 5405.
[33] A. Lipatov, B. B. Wymore, A. Fursina, T. H. Vo, A. Sinitskii, J. G. Redepenning, *Chem. Mat.* **2015**, *27*, 157.
[34] H. O. Pierson, in *Handbook of Carbon, Graphite, Diamonds and Fullerenes* (Ed: H. O. Pierson), William Andrew Publishing, Oxford, **1993**, p. 43.
[35] J. H. Chen, C. Jang, S. Adam, M. S. Fuhrer, E. D. Williams, M. Ishigami, *Nat. Phys.* **2008**, *4*, 377.
[36] C. Gomez-Navarro, R. T. Weitz, A. M. Bittner, M. Scolari, A. Mews, M. Burghard, K. Kern, *Nano Lett.* **2007**, *7*, 3499.
[37] A. Sinitskii, A. A. Fursina, D. V. Kosynkin, A. L. Higginbotham, D. Natelson, J. M. Tour, *Appl. Phys. Lett.* **2009**, *95*, 253108.
[38] D. K. Efetov, P. Kim, *Phys. Rev. Lett.* **2010**, *105*, 256805.
[39] C. R. Dean, A. F. Young, I. Meric, C. Lee, L. Wang, S. Sorgenfrei, K. Watanabe, T. Taniguchi, P. Kim, K. L. Shepard, J. Hone, *Nat. Nano* **2010**, *5*, 722.
[40] F. Chen, J. Xia, D. K. Ferry, N. Tao, *Nano Lett.* **2009**, *9*, 2571.
[41] C. Jang, S. Adam, J. H. Chen, E. D. Williams, S. Das Sarma, M. S. Fuhrer, *Phys. Rev. Lett.* **2008**, *101*, 146805.
[42] A. Lipatov, P. M. Wilson, M. Shekhirev, J. D. Teeter, R. Netusil, A. Sinitskii, *Nanoscale* **2015**, *7*, 12291.
[43] D. B. Asay, S. H. Kim, *J. Phys. Chem. B* **2005**, *109*, 16760.
[44] A. Verdaguer, C. Weis, G. Oncins, G. Ketteler, H. Bluhm, M. Salmeron, *Langmuir* **2007**, *23*, 9699.
[45] L. T. Zhuravlev, *Colloids Surf. A: Physicochem. Eng. Aspects* **2000**, *173*, 1.
[46] H. Ghassemi, W. Harlow, O. Mashtalir, M. Beidaghi, M. R. Lukatskaya, Y. Gogotsi, M. L. Taheri, *J. Mater. Chem. A* **2014**, *2*, 14339.
[47] A. Sinitskii, A. Dimiev, D. A. Corley, A. A. Fursina, D. V. Kosynkin, J. M. Tour, *ACS Nano* **2010**, *4*, 1949.
[48] F. Schedin, A. K. Geim, S. V. Morozov, E. W. Hill, P. Blake, M. I. Katsnelson, K. S. Novoselov, *Nat. Mater.* **2007**, *6*, 652.
[49] H. Liu, Y. Liu, D. Zhu, *J. Mater. Chem.* **2011**, *21*, 3335.
[50] Y. Sato, K. Takai, T. Enoki, *Nano Lett.* **2011**, *11*, 3468.
[51] A. Lipatov, A. Varezhnikov, [illegible]son, V. Sysoev, A. Kolmakov, A. Sinitskii, *Nanoscale* **2013**, [illegible].
[52] A. Lipatov, A. Varezhnikov, M. Augustin, M. Bruns, M. Sommer, V. Sysoev, A. Kolmakov, A. Sinitskii, *Appl. Phys. Lett.* **2014**, *104*, 013114.
[53] M. Naguib, Y. Gogotsi, *Acc. Chem. Res.* **2015**, *48*, 128.
[54] B. Anasori, Y. Xie, M. Beidaghi, J. Lu, B. C. Hosler, L. Hultman, P. R. C. Kent, Y. Gogotsi, M. W. Barsoum, *ACS Nano* **2015**, *9*, 9507.

Q1 APT to AU: Please provide the highest academic title (either Dr. or Prof.) for all authors, where applicable.

Q2 APT to AU: Please insert suitable section headings (e.g., Introduction, Results and Discussion, Conclusion) in this article. These are required for the article type (Full Paper).

Q3 APT to AU: Please define 'PVDF' at the first occurrence in the text.

Q4 APT to AU: Please check subparts in caption of Figure 3 have been typeset as per artwork.

Q5 APT to AU: Please check all equations have been correctly typeset.

Q6 APT to AU: As per journal style, 'Equal Contribution Text' has been moved to the 'Acknowledgements' section. Please check.

Q7 APT to AU: Please provide volume/page numbers in ref. [9] if now available.